

Development of the Laser Altimeter (LIDAR) for Hayabusa2

T. Mizuno^{1,2} · T. Kase³ · T. Shiina³ · M. Mita¹ ·
N. Namiki⁴ · H. Senshu⁵ · R. Yamada⁴ · H. Noda⁴ ·
H. Kunimori⁶ · N. Hirata⁷ · F. Terui¹ · Y. Mimasu¹

Received: 11 August 2015 / Accepted: 23 December 2015 / Published online: 18 February 2016
© Springer Science+Business Media Dordrecht 2016

Abstract Hayabusa2 was launched on 3 December 2014 on an H-IIA launch vehicle from the Tanegashima Space Center, and is, at the time of writing, cruising toward asteroid 162137 Ryugu (1999JU₃). After reaching the asteroid, it will stay for about 1.5 years to observe the asteroid and collect surface material samples.

The light detection and ranging (LIDAR) laser altimeter on Hayabusa2 has a wide dynamic range, from 25 km to 30 m, because the LIDAR is used as a navigation sensor for rendezvous, approach, and touchdown procedures. Since it was designed for use in planetary explorers, its weight is a low 3.5 kg. The LIDAR can serve not only as a navigation sensor, but also as observation equipment for estimating the asteroid's topography, gravity and surface reflectivity (albedo). Since Hayabusa2 had a development schedule of just three years from the start of the project to launch, minimizing development time was a particular concern. A key to shortening the development period of Hayabusa2's LIDAR system was heritage technology from Hayabusa's LIDAR and the SELENE lunar explorer's LALT laser altimeter.

✉ T. Mizuno
tmizuno@isas.jaxa.jp

¹ Japan Aerospace Exploration Agency, 3-1-1 Yoshinodai Chuo-ku, Sagamihara, Kanagawa 252-5210, Japan

² Department of Space and Astronautical Science, School of Physical Sciences, Japan Aerospace Exploration Agency, SOKENDAI (The Graduate University for Advanced Studies), 3-1-1 Yoshinodai Chuo-ku, Sagamihara, Kanagawa 252-5210, Japan

³ NEC Corporation, 1-10 Nisshin-cho, Fuchu, Tokyo 183-8501, Japan

⁴ National Astronomical Observatory of Japan, 2-2-1 Osawa, Mitaka, Tokyo 181-8588, Japan

⁵ Planetary Exploration Research Center, Chiba Institute of Technology, 2-17-1 Tsudanuma, Narashino, Chiba 275-0016, Japan

⁶ National Institute of Information and Communications Technology, 4-2-1 Nukui-kitamachi, Koganei, Tokyo 184-8795, Japan

⁷ Research Center for Advanced Information Science and Technology, University of Aizu, Aizu-wakamatsu, Fukushima 965-8580, Japan

Given that the main role of Hayabusa2's LIDAR is to serve as a navigation sensor, we discuss its development from an engineering viewpoint. However, detailed information about instrument development and test results is also important for scientific analysis of LIDAR data and for future laser altimetry in lunar and planetary exploration. Here we describe lessons learned from the Hayabusa LIDAR, as well as Hayabusa2's hardware, new technologies and system designs based on it, and flight model evaluation results. The monolithic laser used in the laser module is a characteristic technology of this LIDAR. It was developed to solve issues with low-temperature storage that were problematic when developing the LIDAR system for the first Hayabusa mission. The new module not only solves such problems but also improves reliability and miniaturization by reducing the number of parts.

Keywords LIDAR · Laser altimeter · YAG · Hayabusa · Asteroid exploration

1 Introduction

In recent years, many probes have been sent to the Moon, planets, asteroids, and comets to perform scientific observations and search for life. Many of these probes carry light detection and ranging (LIDAR) systems that can measure ranges from tens to hundreds of kilometers. Many LIDAR systems on planetary explorers have produced significant results as orbital remote sensors. Examples of LIDAR carried in probes to the Moon or planets include the LIDAR on the lunar probe Clementine (1994) (Nozette et al. 1994), MOLA on the Mars Global Surveyor (1996) (Ramos-Izquierdo et al. 1994), MLA on Messenger (2004) (Cavanaugh et al. 2007), LALT on SELENE (Araki et al. 2008), LAM on Chang'e-1 (2007) (Huang et al. 2010), LLRI on Chandrayaan-1 (2008) (Kamalakar et al. 2005), and LOLA on the Lunar Reconnaissance Orbiter (2009) (Riris et al. 2007). In addition, BELA (Thomas 2007) has been developed for the ESA Mercury space probe BepiColombo. These LIDAR systems have maximum ranges in the hundreds of kilometers. The NLR systems on NEAR Shoemaker (1996) (Cole et al. 1996) and OLA (Dickinson et al. 2012) on OSIRIS-REx are used for tasks such as geomorphologic mapping of asteroids. OSIRIS-REx is equipped with 3D Flash LIDAR for guidance, navigation, and control (GN&C) before landing.

The LIDARs on Hayabusa (2003) (Mizuno et al. 2006, 2010) and Hayabusa2 (2014) are mainly used as navigation sensors for rendezvous and touchdown. After touchdown, long communication delays (about 40 min both ways) and low bit rates mean that advanced autonomy is required for probe GN&C. To that end, these probes adopt autonomous navigation systems based on LIDAR and cameras. LIDAR is thus an important navigation sensor during asteroid rendezvous, approach, and touchdown. LIDAR is also used for applications such as global topographic mapping, gravity estimation, and reflectance distribution observation. In the Hayabusa mission, scientists successfully used LIDAR measurements to estimate the asteroid's weight and density (Abe et al. 2006).

Range data acquired by the Hayabusa2 LIDAR will be used for scientific analysis of 162137 Ryugu (1999JU₃). First, a shape model will be developed from a combination of camera images and LIDAR range data. A non-dimensional shape is estimated using camera images taken from various angles, and LIDAR range data determine the length scale. The asteroid's gravity, and hence its mass, can be measured from spacecraft tracking data and LIDAR range data when the spacecraft descends toward Ryugu from an altitude of 20 km to 1 km without orbital maneuvers and when the spacecraft ascends freely to the home position (HP). Such gravity experiments will be conducted two to six times to improve the accuracy of gravity and rotational axis measurements. The measured mass and the volume estimated

from the shape model will provide the density of Ryugu within an accuracy of 10 %, constraining the internal structure of Ryugu. LIDAR measures not only ranges but also the intensity of transmitted and received laser pulses. LIDAR is an active sensor, unlike other instruments aboard Hayabusa2, and the ratio of transmitted and received energy can be translated into normal albedo on the surface of Ryugu. We take advantage of the wide dynamic range of the Hayabusa2 LIDAR to detect dust possibly lofting above the asteroid's surface. A new function called "dust count" is implemented on the Hayabusa2 LIDAR to observe the spatial distribution of dust density in eight levels with a resolution of 20 m along the line of sight direction.

Hayabusa weighed about 500 kg, making it relatively lightweight compared with other explorers. Because of the severe system weight restrictions, the LIDAR was designed to have low weight (3.7 kg) in addition to large dynamic range. The Hayabusa2 LIDAR has newly added functions for measuring surface reflectance and surface dust observation, and a transponder for laser ranging (Noda et al. 2013). Also of note is that the LIDAR was developed quickly, with just three years from the start of the project to launch.

This paper describes in detail the role of the Hayabusa2 LIDAR system as a GN&C navigation sensor and science instrument (Sect. 2), the hardware used (Sect. 3), technical decisions for shortening the development time (Sect. 4), and system evaluation results (Sect. 5). We will frequently compare the LIDAR on Hayabusa with the one on Hayabusa2; note that mentions of "the LIDAR" below without explanation indicates the LIDAR on Hayabusa2.

2 Rendezvous and Touchdown Sequence

Hayabusa2 will approach asteroid Ryugu using an orbital determination by conventional range and range rate (R&RR) and delta-differential one-way ranging (DDOR) to a detectable distance by an optical navigation camera (ONC). A star tracker can be used instead of an ONC. Hayabusa2 is guided by R&RR and optical navigation (OPNAV) (Terui et al. 2013) using ONC images to approach to 25 km. Range-finding by LIDAR becomes possible at distances of 25 km or less. The orbit around the target asteroid is determined using asteroid-explorer range-finding by LIDAR and Earth-explorer range-finding by R&RR from ground stations. The effect of gravity can be ignored beyond about 20 km from the asteroid, and we nominally choose this as the HP of the spacecraft for global mapping (GM). The explorer will remain at the HP using home position navigation (HPNAV) control, and will perform image acquisition by ONC and GM by LIDAR using rotation of the asteroid. On the basis on these data, the project team will select candidate points for touchdown and form a touchdown plan.

In the touchdown sequence, the explorer will descend from the HP to an altitude of about 50 m by ground control point navigation (GCPNAV) control. A target marker will be released from an altitude of 30–50 m to determine the final sampling point. The target marker reflects light from a flash lamp on the explorer to show the ONC the landing point. Finally, the explorer will land from an altitude of 50 m or less by autonomous navigation using the target marker and a laser rangefinder with four beams. The ONC will continuously transmit pictures to the ground during the descent. Operators will use these images to determine whether the descent is proceeding as planned and thereby make a proceed/abort judgment and determine final compensation delta-V commands.

LIDAR plays an important role not only as a range sensor for navigation but also as a science instrument for acquisition of data on topography, surface albedo, gravity, and dust

distribution. During the touchdown sequence described above, the diameter of the footprint decreases as the spacecraft approaches the asteroid, providing a unique opportunity to produce high-resolution local models of an asteroid’s topography and surface albedo. The touchdown sequence is also of particular importance for the gravity experiment; while interactions with the solar wind will govern perturbations of the spacecraft’s orbital motion at altitudes higher than 20 km, the gravity of the asteroid will control free-fall and free-rise motion at altitudes lower than 5 km. A precise orbit determination below 5 km altitudes is thus crucial for estimating the asteroid mass. The touchdown sequence is also important for the dust count, because the intensity of laser pulses reflected by the dust cloud increases as the observation altitude decreases. Detection of the return pulse from a thin dust cloud whose intensity is close to threshold levels will only be possible during the touchdown sequence.

3 LIDAR System

3.1 LIDAR Ranges

The LIDAR on Hayabusa2 must permit range-finding over 25 km to 30 m from Ryugu. We briefly describe the radar budget in this range. Assuming the asteroid surface is a Lambertian target, the received energy P_r from a distance R is given by

$$P_r = \frac{\tau D_r^2 \rho_t}{4R^2} P_t \times \text{overlap}(R) \tag{1}$$

Here, τ is the transmissivity of the optics, D_r is the diameter of the receiver optics, R , is the range, P_t is the transmitted energy, and ρ_t is the target surface albedo. Overlap(R) is a function giving the field-of-view (FOV) overlap rate of the transmitted beam and receiving telescope. However, the function is complicated, because it can be purely decided geometrically from FOV of the transmitted beam and the receiving telescope, and their arrangement. Thus, we do not describe it here. In consideration of the alignment offset seen in the heat vacuum test described in Sect. 5.2, we take the overlap to be 0.35 at large distances. The FOV of the receiving telescope is sufficiently large at short distances that it is unnecessary to consider it. Figure 1 shows the relation between received energy and distance. The timing detection threshold of the receiving circuit for the ranging mode is 30 mV, which is sufficiently higher than the noise floor. In this case, because the sensitivity of the avalanche photodiode–hybrid IC (APD-HIC) reception is 500 kV/W, the minimum detectable level is 6×10^{-8} W. From Fig. 1, we can see that the LIDAR can make measurements at a distance

Fig. 1 LIDAR link budget. Here, the transmitted energy P_t , reflectance ρ_t , and laser beam divergence angle are 15 mJ, 0.06, and 2.5 mrad, respectively. Telescope parameters D_r , τ , and FOV have respective values of 110 mm, 0.678, and 1.5 mrad at large distances and 3 mm, 0.728, and 20 mrad at short distances. The function $\text{overlap}(R)$ is taken to be 0.35 at large distances

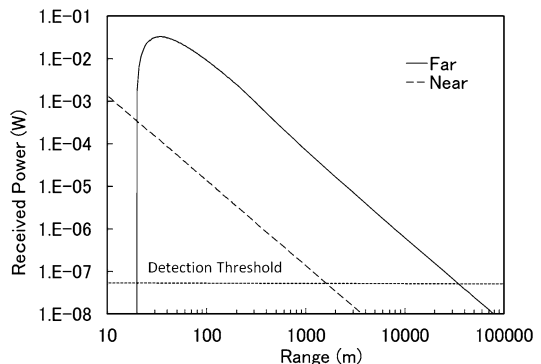


Fig. 2 Photograph of the FM LIDAR

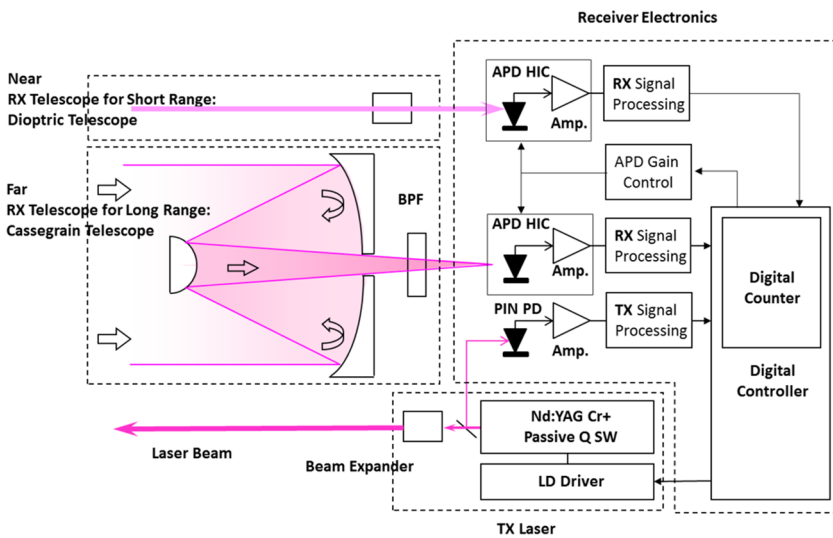


Fig. 3 LIDAR system block diagram

over 30 km. When the inclination of a geographical feature in the laser beam footprint is large, it is necessary to take into consideration that the reflected pulse width is increased by the feature’s altitude difference.

3.2 Outline of Hayabusa2 LIDAR

Figure 2 shows the photograph of the flight model of LIDAR and Fig. 3 illustrates the system block diagram of the LIDAR system. The design of the chassis, baffle, and radiator are unchanged, so the system has the same appearance as the Hayabusa LIDAR. The LIDAR system is a pulse radar that uses a YAG laser (fundamental wavelength: 1064 nm) as a transmitting light source, and it measures distances by measuring the time-of-flight (TOF) of the laser pulse.

As shown in the block diagram in Fig. 3, the LIDAR consists of a laser module, a telescope that receives reflected pulses, and a digital controller that controls the laser and mea-

Table 1 Main specifications of the LIDAR

Range	30 m–25 km (expected albedo: 0.06–0.1)
Resolution	0.5 m
Accuracy (1σ)	± 1 m (at 30 m) < ± 5.5 m (at 25 km)
Repetition rate	Driven by an external trigger. Max. 1 Hz
Laser transmitter	Monolithic passive Q-SW Nd:YAG + Cr Wavelength: 1064 nm; Pulse energy: 15 mJ; Pulse width: 7 ns
Receiver optics	Long range (>1 km): effective diameter: 110 mm (Cassegrain, SiC); FOV: 1.5 mrad Short range (<1 km): effective diameter: 3 mm, FOV: 20.4 mrad
Receiver detector	Si APD-HIC
Telemetry data	17-bit range data (equivalent to 65 km) Monitors for the transmitting laser energy and received signal energy Hardware statuses 10 words (1 word = 16 bits).
Electrical interfaces	Voltage: +30.5–51 V Power consumption: 18 W Communication: RS422
Mechanical interfaces	Dimensions: 241 × 228 × 229 mm Weight: 3.52 kg (including DC/DC, radiator)
Thermal interfaces	Storage temperature: –30 to +60 °C Operating temperature: +10 to +40 °C

sure the TOF. Table 1 lists the main specifications. One feature of this LIDAR is that it has two receiving systems: one for long-range measurements and one for short-range measurements. We call the long-range system “Far” and the short-range system “Near.” Due to differences in their apertures, the light energy received by the Near system is 1/1345 that received by the Far system. This difference in light energy compensates for the poor dynamic range of the APD sensor circuit, described in detail in Sect. 3.4.2. The dynamic range of the LIDAR is wide, from 30 m to 25 km. The ranging accuracies required for GN&C are 1 m and 5.5 m at minimum and maximum distances, respectively. The ranging resolution is 0.5 m. The LIDAR is operated by ranging request commands from the attitude control system (AOCS), and both the repetition rate of the transmitting laser and the data refresh rate are 1 Hz at maximum.

From the perspective of scientific analysis of range data, the requirements for the LIDAR performance are summarized as follows. First, requirements for global topographic mapping from the HP are (i) a range counter larger than 17 bits, (ii) a laser transmission energy stronger than 10 mJ, and (iii) distribution of transmitted energy within the FOV of receiver optics larger than 21 %. In addition, requirements for producing a shape model with an estimation error less than 10 m in radial topography are (iv) a range accuracy better than 5.5 m, and (v) range resolution along the line of sight better than 1 m. Among these requirements, (i) was satisfied by the telemetry design; the remaining items were evaluated during a series of tests. Other requirements related to albedo measurement and dust detection, respectively, are described and evaluated in companion papers by Yamada et al. (2016, [this issue](#)) and Senshu et al. (2016, [this issue](#)).

Fig. 4 Photograph of the BBM laser module

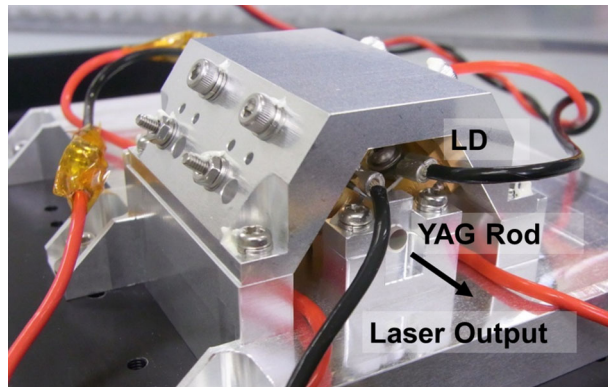
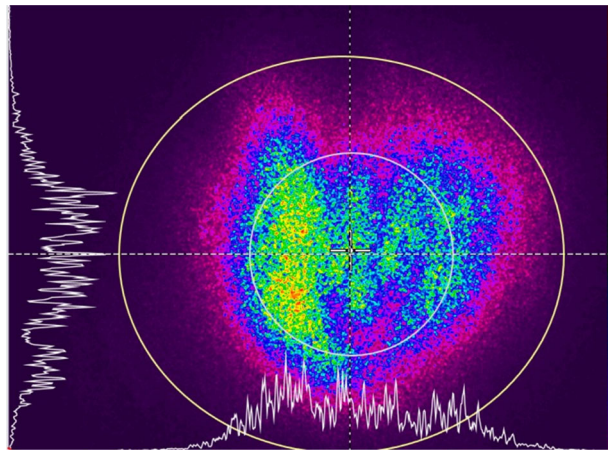


Fig. 5 Beam profile of the FM laser



3.3 Transmitter

As described in Sect. 4, the laser is based on the ones used in Hayabusa and SELENE, and is a characteristic technology of this LIDAR. Figure 4 shows a photograph of the breadboard model (BBM) of laser module. The laser resonator has a monolithic structure with a mirror coating at the both ends of a YAG rod with Cr co-dopant. The YAG rod ($\phi 3 \times 40$ mm) has a layer of Cr^{4+} saturable absorber on one side as a passive Q-switch. The resonator of Hayabusa's LIDAR comprised 13 optical components: two wedge plates, two wavelength plates, three protection windows, a Pockels cell crystal, the YAG rod, the polarizing plate, two prisms, and the output mirror. These optical components were united into one rod in the laser module of Hayabusa2. The new LIDAR therefore significantly improves robustness to alignment, mechanical vibration, and thermal modification. The laser module is not shielded by a pressure vessel.

The adjusted power of the laser in the flight model (FM) is 15 mJ. However, as Fig. 5 shows, the beam profile is divided into two by multi-mode oscillation. The beam divergence angle after beam expander ($\times 3$) passage was 2.4 mrad. Presumed causes are the heterogeneity of the dopant in the rod, the irradiation angle of laser diode (LD) light, and the concentration of the saturable absorber, and the mirror reflectance can be considered.

Since the radar budget calculation in Sect. 3.1 indicates that the LIDAR range cannot be maintained with less than 35 % of the energy of the transmitting laser, we prioritized keeping to the development schedule over improving the laser and left this shortcoming as a point for improvement in future development. The decline in energy availability in oscillation mode had a big effect on albedo observation. Change of the shot-by-shot availability factor was evaluated in detail by Yamada (Yamada et al. 2016, [this issue](#)).

Regarding the LD life, we confirmed no LD degradation after 16,320,000 LD shots using the same lot as the FM parts, operating at 1 Hz in vacuum. We prepared for unexpected output degradation as experienced by the lunar probe SELENE by implementing a function to adjust the LD excitation current pulse width via commands from the ground. The adjustable range is from 45 to 300 μs . When the LDs maintain their initial output at room temperature, the YAG laser can generate a pair of double pulses by means of LD drive current with a pulse width of 115 μs or more.

3.4 Receiver

3.4.1 Optics

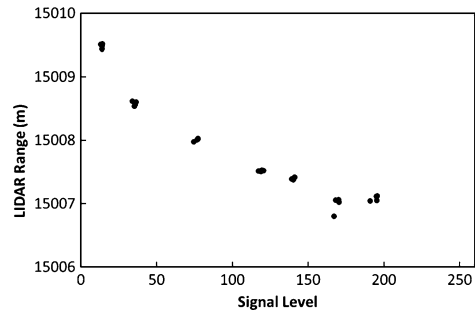
As described in Sect. 3, the LIDAR has two receiving systems: the Far optics for long distances and Near optics for short distances. The received light level of the Far optics is 1345 times that of the Near optics, allowing the LIDAR to perform measurements over a wide dynamic range. The Far telescope consists of relay optics and a Cassegrain telescope that has an effective diameter of 110 mm and focal length of 1200 mm (Table 1). The relay optics has a 5-nm band-pass filter mounted for background light reduction. The Cassegrain telescope's main reflector, sub-reflector, and sub-reflector support are manufactured using new-technology silicon carbide (NT-SiC) as the main material. Gold vapor deposition is used for the optical specular surface. Since the LIDAR is used during touchdown, it receives thermal radiation directly from the asteroid. Silicon carbide was adopted to minimize modification by this temperature change. The same material was used for Hayabusa. The Near telescope is a dioptric system with a small (3 mm) effective diameter and a 5 nm filter.

3.4.2 Sensor and Circuit

To shorten the development period, we used a heritage receiving circuit adopted from an HIC by Excelitas Technologies Corp. for the LALT on SELENE. The HIC contains a transimpedance pre-amplifier and an APD in one package. However, since the gain of the pre-amplifier is fixed, it cannot cover the dynamic range demanded by Hayabusa2. Even adjusting the APD multiplication factor M would give at most 20 dB, and the frequency response would be extremely slow if the multiplication factor were set to 1 by zero bias. Because a dynamic range of 60 dB cannot be covered with such gain adjustments, we permitted saturation of the amplifier output at distances where reflectance measurements are not needed. Range-finding is thus possible even when amplifier output is saturated.

Figure 6 shows the relation between the measured distance and the received signal level (0–255) that appears in telemetry. In this examination, a delayed electrical signal equivalent to 15,000 m was inputted at room temperature. This result shows that ranging results can differ by around 3 m, depending on the received signal level. In the LIDAR, this distribution is approximated by a linear function. A correction coefficient for temperature has also been determined.

Fig. 6 Dependence of received signal level on measured distance



The gain can be changed in four steps by selecting the Near or Far optics and changing the APD multiplication factor M . The highest gain is obtained by a combination of Far with $M = 100$ (high). The fourth gain setting, the lowest gain, is obtained by combination of Near and $M = 10$ (low). Assuming the highest gain to be 1.0, the second, third, and fourth gains are respectively 0.1, 0.000743, and 0.0000743. The bandwidth of the receiving circuit is 100 MHz, sufficient to detect the leading edge of a received pulse.

Although the gain can be set by manual commands, automatic gain control (AGC) is used during the touchdown sequence. The intensity of the transmitting laser and received signal are important information for determining the surface albedo and performing health checks. The LIDAR detects the timing and peak of the transmitting laser using a PIN photodiode (PIN-PD). The output from the PIN-PD is integrated, and the peak is read as transmission output. The timing and peak of the received pulse is also detected. To measure the albedo of the asteroid surface, in addition to calibrating the gain as described above, we also need to calibrate the thermal dependence of the alignment offset with the transmission-reception alignment. The influence of this alignment on albedo measurement is estimated in detail by Yamada et al. (2016, [this issue](#)).

3.5 Digital Controller

3.5.1 Ranging Function

The LIDAR has the three operational modes: ranging mode, optical link (transponder) mode, and dust count mode. In ranging mode, the digital controller handles laser shots, reflected pulse detection, and telemetry transmission.

This operation is carried out synchronously with commands from the AOCS. The repetition rate of the ranging command must be 1 Hz or less. Since the transmitting laser of this LIDAR has a passive Q-switch, the timing of each shot has jitter for hundreds of nanoseconds. The laser transmission timing is detected by the PIN-PD, and the receiving timing of the reflected pulse is detected by the APD-HIC. LIDAR sends transmissions and reception time tags to the AOCS as telemetry, and the AOCS calculates the distance from the TOF. The controller operates at 300 MHz and the distance resolution is 0.5 m.

3.5.2 Transponder Function

The LIDAR transponder function transmits a laser pulse immediately after receiving a laser pulse. This is called the “triggered response transponder” function. The time from transmission to reception is measured and sent to the ground as telemetry data. We are planning a

laser ranging experiment using this transponder function between Hayabusa2 and a ground station used for satellite laser ranging (SLR) (Noda et al. 2013). The SLR experiment requires pointing the LIDAR toward Earth. For safety, the mother ship needs to maintain sufficient solar cell power generation, so the Sun–probe–Earth angle formed needs to be 120° or more. Under the present orbital plan, this condition will be fulfilled about two months before and after Earth swing-by. At that time, the distance from Earth to Hayabusa2 will be 10 million kilometers or less.

The LIDAR has a transponder function to return responder pulses, responding to a laser pulse from a ground station as an interrogator. In transponder mode, the LIDAR opens the receiving gate and waits for a laser pulse. If a laser from the ground station is received, the LIDAR will transmit the laser immediately. This receiving time and the laser transmitting time are sent by the usual communications link as telemetry data. The TOF is measured using a highly precise ground-based clock system. Therefore, the “triggered response transponder” function for SLR can be implemented using a simple clock system on the spacecraft. The LIDAR can respond to both single and double pulses from the ground station. When a double pulse is used, we can calibrate the LIDAR counter by measuring the double pulse interval at both the LIDAR and the ground station. The LIDAR transmits a single pulse even when a double pulse is received.

3.5.3 Dust Count Function

According to one hypothesis, dust may be floating near the poles on the surface of the asteroid. To observe this, the LIDAR has a dust count function whereby the distribution of dust in the range of 1 km with the spatial accuracy of 20 m along its view direction. However, the function cannot detect the reflection intensity. Although the measurement length (1 km) is fixed, the measurement position can be changed with a command (Senshu et al. 2016, [this issue](#)).

4 Shortening the Development Period

4.1 Lessons Learned

The transmitting laser of Hayabusa’s LIDAR employed an active Q-switch and a Nd:YAG laser (wavelength of $1.064 \mu\text{m}$ with LD pumping). A Pockels cell (LiNbO_3) crystal was used as the active Q-switch. However, in thermal vacuum tests of the laser module, the output power of the laser decreased when the laser temperature was decreased to 10°C or less. We also found a fault in which laser output did not recover even after returning to room temperature, due to degradation of the extinction ratio of the Pockels cells (Mizuno et al. 2006).

It is known that the LD in a high-power quasi-continuous wave laser will deteriorate with the number oscillations, thus decreasing output; generally speaking, an LD’s useful lifetime is about 10^9 shots. In the case of the LALT on SELENE, however, laser power began to rapidly decrease at about 10^7 shots in orbit, even though the laser power was maintained over 10^8 shots in preflight tests. We attributed this to deterioration of LD output (Araki et al. 2008). This phenomenon was not observed in Hayabusa’s LIDAR.

The Hayabusa LIDAR receiver used a charge amplifier as a pre-amplifier. Charge amplifier output was converted into a bipolar pulse using a pulse-shaping amplifier, and a comparator detected the zero-crossing point for signal timing. In accordance with adjustment of

the APD reverse-bias voltage, there were eight gain steps. By gain adjustment, the output of the preamplifier was not saturated from 50 km to 50 m.

This was satisfactory for AGC operations in orbit but problematic in that circuit adjustments on the ground took too long. Furthermore, there was a lack of personnel with the required know-how on the Hayabusa2 team. In the case of the LALT on SELENE, a wide dynamic range was not needed for mapping from orbit, so the LALT used an HIC equipped with a transimpedance amplifier with fixed gain and an APD.

4.2 Development Scheduled and Time-Saving Measures

The Hayabusa2 project officially started in 2012. Asteroid Ryugu was selected as the asteroid for landing with a launch window of early of December 2014, leaving only three years for development of the FM. Regarding the LIDAR, the receiving circuit BBM and a prototype Cassegrain telescope were manufactured in 2012 and then engineering model (EM) manufacturing was started. While starting manufacture of the FM in 2013, evaluation testing of the EM was performed and the results were fed back to the FM. FM manufacturing was completed late in 2013. The LIDAR was added to the FM comprehensive test in early 2014.

Below we discuss some of the technical decisions made to complete manufacture under such a tight development schedule. Because of the short development period, Hayabusa2's LIDAR inherited its fundamental design from the one used on Hayabusa. However, as described in Sect. 4.1 there were some problems with Hayabusa's LIDAR. The chassis, radiator, and receiving telescope baffle were adopted without change, because their weight had already been thoroughly reduced. In the case of the Cassegrain telescope, a production stoppage caused the material to be changed to a similar kind of silicon carbide, but the design was unchanged.

We needed to cope with several problems related to the laser. Namely, (1) its vulnerability to temperature change, (2) its vulnerability to mechanical stress, and (3) degradation of the LD. To solve (1), in 2007 we developed a YAG laser with a passive Q-switch using a "Cr⁴⁺:YAG" saturable absorber. This laser resonator has a monolithic structure that incorporates the mirror and the saturable absorber into a single rod-shaped body (Kase et al. 2012). We solved the vulnerability to temperature change by adopting a passive Q-switch instead of a Pockels cell, which is sensitive to temperature. In addition, the monolithic structure of the resonator solved problem (2), vulnerability to mechanical stress. This development furthermore decreased the dimensions of the laser from 100 × 150 × 50 mm to 66 × 90 × 40 mm.

We attained a -40 °C lower limit for the laser preservation temperature. Regarding problem (3), degradation of the LD, we were unable to identify the exact cause of the degradation. So, we prepared a function that lengthens the pulse width of the LD excitation current on command using characteristics of the passive Q-switch. If the LD output declines, this function can supply oscillation energy by lengthening the excitation current pulse.

Because of our heritage technology and the very short development period, the receiver's sensor and amplifier adopted the same HIC (Excelitas Technologies Corp.) used for SELENE. However, since that HIC has a fixed-gain amplifier, it cannot cover the required wide dynamic range (25 km to 30 m). We therefore prepared two optical systems.

One system is the Cassegrain telescope, which measures long distances (1–25 km), and the other is a telescope with a small aperture for measuring short distances (less than 1 km). Furthermore, it was necessary for the HIC amplifier output to allow saturation at some distances. By adopting this HIC, we shortened the development period by using a heritage circuit from the SELENE LALT. Since the amplifier is saturated at ranges of 30 m to hundreds of meters and from 1 km to several kilometers, the LIDAR cannot measure the intensity of

a received pulse at these distances. Although the AGC is slightly complicated due to the use of two optical systems, one merit is that we have a redundant system near 1 km.

5 Evaluation Results

5.1 Ranging Function

This section describes some pre-flight tests of the FM LIDAR. Figure 7 shows the results of evaluating the ranging circuit of the long-distance Far and the short-distance Near optics using delayed LD pulses. The evaluation equipment detects transmitted laser pulses using a PIN-PD, and then generates a delayed light pulse using an LD attached to the receiving telescope. Therefore, the received signal level of the LIDAR does not change. The horizontal axis shows distance (setting delay time), and the vertical axis shows the measurement distance and its ranging error. The ranging error is the sum of random error (standard deviation) and systematic error (bias). We can see that the LIDAR can measure correct distances over a range of 30 m to 60 km with error of 0.5 m or less. Both Near and Far systems were examined for distances between 1 km and 10 km.

We examined outdoor ranging using EM to check the LIDAR system operations. In this field experiment, we mainly evaluated the AGC operation, optics FOV, and received signal level. Although field experiments are useful for examining overall operation, we must pay attention to airborne dust in the light path, especially at short distances, because this examination was performed in the atmosphere.

Figure 8 shows an example of results from a field test of AGC operation in the Near optical range. In this experiment, the target was a standard diffusion plate (Spectralon) with 10 % reflectance and dimensions of 600×600 mm. LIDAR EM measured the distance to the moving target. The intensity of the transmitting LIDAR laser was adjusted with a neutral-density filter. In the figure, the horizontal axis shows relative time, the left vertical axis shows the received signal level (preamplifier output), and the right vertical axis shows the range. From this figure, we see that the target approached from distances of 100 m to 60 m. This result shows that the LIDAR gain setup correctly changed from Near High to Near Low at 402 s. Before 402 s, the gain was changed to Near Low a few times because the level was saturated, but then returned to Near High because of their poor received signal level. Therefore, it was confirmed that the AGC functioned correctly.

Fig. 7 LIDAR ranging characteristic. “Near Avg.” and “Far Avg.” indicate average values of more than 60 shots. “Near Error” and “Far Error” are standard deviations

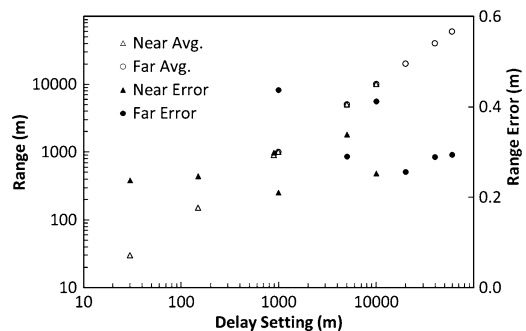


Fig. 8 Evaluation of AGC operation. LIDAR operated by the Near optics for short distances. “Gain H” is the multiplication factor of APD $M = 100$, and “Gain L” is $M = 10$

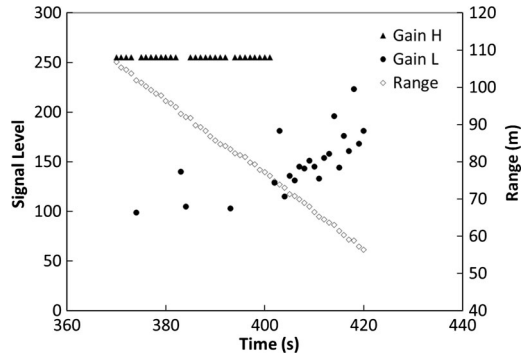
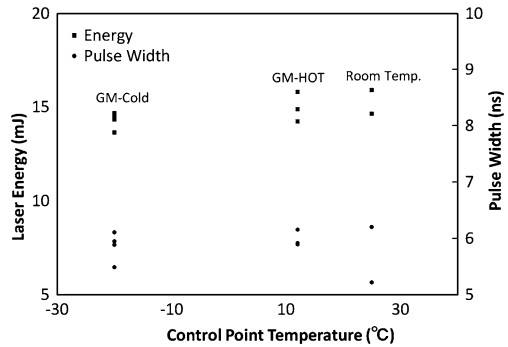


Fig. 9 Temperature dependence of laser energy on pulse width



5.2 Thermal Vacuum Test

Thermal vacuum testing is important for simulating and evaluating operation in the thermal environment of space. For the LIDAR, we conducted thermal vacuum testing to confirm operation after storage at low temperature in the GM and touchdown phases. In the examination, the LIDAR was set on a temperature-controlled board in a vacuum chamber. The inner side of the vacuum chamber was covered by a shroud, which was cooled to $-180\text{ }^{\circ}\text{C}$. We directed the laser output toward an optical window in the chamber and measured the laser energy, beam profile, and transmission-reception optics alignment. The ranging operation was examined with the same equipment (a delayed light pulse by an LD) described in Sect. 5.1.

Figure 9 shows the results of measuring the laser output and pulse width at the upper limit (GM-HOT) and lower limit (GM-COLD) of the specified point temperatures expected to be encountered in the GM phase. The LIDAR was placed under GM-HOT and GM-COLD temperature conditions several times. The average value of data collected over about 1 min is plotted as one point. The room temperature data are measurement results under atmospheric pressure before and after the vacuum test.

We can see that the laser operated without problems under both GM-HOT and GM-COLD conditions; the laser output was stable at 14–15 mJ and the pulse width was a stable 6 ns. In the touchdown phase, laser oscillation can fail due to thermal radiation from the asteroid. The reason for this phenomenon is that the absorption efficiency in the YAG rod decreases due to the changing oscillating wavelength of the LD. For this reason, we lengthen the LD excitation pulse before going into the touchdown phase.

6 Conclusion

Although the development period for Hayabusa2 was a very short three years, we succeeded in its development while incorporating new technologies into the design. Regarding the development of the LIDAR system, shortening the development period was the most important judgment criterion. In this paper, we introduced some examples of utilizing the heritage technology from the Hayabusa asteroid explorer and the SELENE lunar explorer to develop Hayabusa2's LIDAR. We also described the LIDAR hardware and evaluation results in detail. These results show that the requirements are well satisfied for both navigation and asteroid science. In addition to contributing as a navigation sensor to the success of the sample return mission, this LIDAR is expected to contribute to scientific observations and new SLR experiments.

References

- S. Abe, T. Mukai, N. Hirata, O.S. Barnouin-Jha, A.F. Cheng, H. Demura et al., Observing 25143 Itokawa using the light detection and ranging instrument (LIDAR) on the Hayabusa spacecraft: local topography and mass. *Science* **41**(312), 1344–1347 (2006)
- H. Araki, S. Tazawa, H. Noda, T. Tsubokawa, N. Kawano, S. Sasaki, Observation of the lunar topography by the laser altimeter LALT on board Japanese lunar explorer SELENE. *Adv. Space Res.* **42**(2), 317–322 (2008)
- J.F. Cavanaugh, J.C. Smith, X. Sun, A.E. Bartels, L. Ramos-Izquierdo, D.J. Krebs, J.F. McGarry, R. Trunzo, A.M. Novo-Gradac, J.L. Britt, J. Karsh, R.B. Katz, A.T. Lukemire, R. Szymkiewicz, D.L. Berry, J.P. Swinski, G.A. Neumann, M.T. Zuber, D.E. Smith, The mercury laser altimeter instrument for the MESSENGER mission. *Space Sci. Rev.* **131**(1–4), 451–479 (2007)
- T.D. Cole, M.T. Boies, A.S. El-Dinary, Laser radar instrument for the Near-Earth Asteroid Rendezvous (NEAR) mission. *Proc. SPIE Int. Soc. Opt. Eng.* **2748**, 122–139 (1996)
- C.S. Dickinson, M. Daly, O. Bar-nouin, B. Bierhaus, D. Gaudreau, J. Tripp, M. Ilnicki, A. Hildebrand, An overview of the OSIRIS REX laser altimeter—OLA, in *43rd Lunar and Planetary Science Conference* (2012)
- Q. Huang, J.S. Ping, M.A. Wicczorek, J.G. Yan, X.L. Su, Improved global lunar topographic model by Chang'E-1 laser altimetry DATA, in *41st Lunar and Planetary Science Conference* (2010)
- J.A. Kamalakar, K.V.S. Bhaskar, A.S. Laxmi Prasad, R. Ranjith, K.A. Lohar, R. Venketeswaran, T.K. Alex, Lunar ranging instrument for Chandrayaan-1. *J. Earth Syst. Sci.* **114**(6), 725–731 (2005)
- T. Kase, T. Shiina, T. Imaoku, Y. Asakawa, T. Mizuno, Development of the laser oscillator for HAYABUSA2-LIDAR, in *30th Laser Sensing Symposium D-1*, Shodoshima (2012)
- T. Mizuno, K. Tshuno, E. Okumura, M. Nakayama, LIDAR for asteroid explorer Hayabusa: development and on board evaluation. *J. Jpn. Soc. Aeronaut. Space Sci.* **54**(634), 514–521 (2006)
- T. Mizuno, K. Tsuno, E. Okumura, M. Nakayama, Evaluation of LIDAR system in rendezvous and touch-down sequence of Hayabusa mission. *Trans. Jpn. Soc. Aeronaut. Space Sci.* **53**(179), 47–53 (2010)
- H. Noda, T. Mizuno, H. Kunitomi, H. Takeuchi, N. Namiki, Alignment measurement with optical transponder system of Hayabusa2 LIDAR, in *18th International Workshop on Laser Ranging*, 13-Po06, Fujiyoshida (2013)
- S. Nozette, P. Rustan, L.P. Pleasance, J.F. Kordas, I.T. Lewis, H.S. Park, R.E. Priest, D.M. Horan, P. Reagan, C.L. Lichtenberg, E.M. Shoemaker, E.M. Eliason, A.S. McEwen, M.S. Robinson, P.D. Spudis, C.H. Acton, B.J. Buratti, T.C. Duxbury, D.N. Baker, B.M. Jakosky, J.E. Blamont, M.P. Corson, J.H. Resnick, C.J. Rollins, M.E. Davies, P.G. Lucey, E. Malaret, M.A. Massie, C.M. Pieters, R.A. Risse, R.A. Simpson, D.E. Smith, T.C. Sorenson, R.W. Vorder Breugge, M.T. Zuber, The Clementine mission to the Moon: scientific overview. *Science* **266**, 1835–1839 (1994)
- L. Ramos-Izquierdo, J.L. Bufton, P. Hayes, Optical system design and integration of the Mars observer laser altimeter. *Appl. Opt.* **33**(15), 307–322 (1994)
- H. Riris, X. Sun, J.F. Cavanaugh, G.B. Jackson, L. Ramos-Izquierdo, D.E. Smith, M. Zuber, The Lunar Orbiter Laser Altimeter (LOLA) on NASA's Lunar Reconnaissance Orbiter (LRO) mission, in *Proceedings SPIE—The International Society for Optical Engineering*, vol. 6555 (2007), p. 65550
- H. Senshu, S. Oshigami, M. Kobayashi, R. Yamada, N. Namiki, T. Mizuno, Hayabusa2 LIDAR science team, dust detection mode of Hayabusa2 LIDAR. *Space Sci. Rev.* (2016, this issue)

- F. Terui, N. Ogawa, Y. Mimasu, S. Yasuda, M. Uo, Guidance, navigation and control of Hayabusa2 in proximity of an asteroid, in *36th Annual American Astronautical Society Guidance & Control Conference*, AAS 13-094, Colorado (2013)
- N. Thomas, The BepiColombo laser altimeter (BELA): concept and baseline design. *Planet. Space Sci.* **55**, 1398–1413 (2007)
- R. Yamada, H. Senshu, N. Namiki, T. Mizuno, S. Abe, F. Yoshida, H. Noda, N. Hirata, S. Oshigami, H. Araki, Y. Ishihara, K. Matsumoto, Performance of Hayabusa2 LIDAR to observe normal albedo on the C-type asteroid. *Space Sci. Rev.* (2016, this issue)